Chapter 19

ELECTROMAGNETIC WAVE PROPAGATION IN THE LOWER ATMOSPHERE

Section 19.1 V. J. Falcone, Jr.
Section 19.2 R. Dyer

19.1 REFRACTION IN THE LOWER TROPOSPHERE

The speed of propagation of an electromagnetic wave in free space is a constant, c, which is equal to 3×10^8 m/s. In a material medium such as the atmosphere, the speed of propagation varies. Even small variations in speed produce marked changes in the direction of propagation, that is, refraction.

In the atmosphere, the speed of propagation varies with changes in composition, temperature, and pressure. At radio wavelengths, speed does not vary significantly with the wavelength, but in the optical region the speed depends strongly on the wavelength. In the lower 15 km of the atmosphere, water vapor is the most highly variable of the atmospheric gases, and at radio wavelengths the speed of propagation is strongly affected by water vapor. Temperature and pressure variations are principally functions of altitude, although for propagation at small elevation angles significant variations may occur along horizontal distances. From the standpoint of effect on the speed of propagation, temperature variations at any given altitude are more significant than pressure variations.

In its most general form, the refractive index is a complex function. The real term of the complex function is called the *phase refractive index*, n;

$$n = \frac{c}{v} \tag{19.1}$$

where c is the speed of light in a vacuum and v, the *phase velocity*, is the speed of propagation in a particular medium. In the troposphere where n is nearly equal to one, it is convenient to define the quantity

$$N = (n - 1) \times 10^6. \tag{19.2}$$

N is called the *refractive modulus*; units of $(n - 1) \times 10^6$ are called N-units.

19.1.1 Optical Wavelengths

An approximate relation between the optical refractive modulus and atmospheric pressure and temperature is

$$N_\infty = 77.6 \frac{P}{T} \tag{19.3}$$

where N_∞ is the refractive modulus for wavelengths $\gg 20$ μm, P is atmospheric pressure in millibars, and T is atmospheric temperature in degrees kelvin.

The dispersion formula of Edlen [1953], which has been adopted by the Joint Commission for Spectroscopy, is

$$N_s = 64.328 + \frac{29498.10}{146 - 1/\lambda^2} + \frac{255.40}{41 - 1/\lambda^2}, \tag{19.4}$$

where N_s is the refractive modulus at a wavelength λ for a temperature of 288 K and a pressure of 1013.25 mb, and λ is the wavelength in micrometers. A somewhat less precise but more convenient dispersion formula is

$$N = N_\infty \left[1 + \frac{7.52 \times 10^{-3}}{\lambda^2}\right]. \tag{19.5}$$

Equations (19.3) and (19.5) can be combined to give the refractive modulus as a function of pressure, temperature, and wavelength;

$$N = \frac{77.6\ P}{T} + \frac{0.584\ P}{T\ \lambda^2}. \tag{19.6}$$

Refractive moduli calculated by using Equation (19.6) will be in error no more than one N-unit over the temperature range 243 to 303 K for wavelengths from 0.2 to 20 μm. Thus Equation (19.6) covers the spectrum from the far ultraviolet through the near infrared. A more accurate relationship is given in Chapter 18.

19.1.2 Radio Wavelengths

At radio wavelengths the relationship of refractive modulus to pressure, temperature, and water-vapor pressure is given by

$$N = \frac{77.6P}{T} + \frac{373000P_{wv}}{T^2}, \qquad (19.7)$$

where P_{wv} is the partial pressure of water vapor in millibars, P is pressure in millibars, and T is temperature in degrees kelvin. Equation (19.7) is accurate to 0.1 N-unit from the longest radio wavelengths in use down to about 6 mm (50 GHz); 5 N-units from 6 to 4 mm (50 to 75 GHz); and 1 N-unit from 4 to 2.6 mm (75 to 115 GHz). A more accurate description of refraction and its effects in the 30 to 1000 GHz region (EHF range) has been investigated by Liebe [1980].

Absorption by atmospheric constituents begins to rise to significant proportions with decreasing wavelength beginning near 1.5 cm. Water vapor content is by far the leading factor in causing changes in N, followed in order of importance by temperature and pressure. For example, for a temperature of 288 K, pressure of 1013 mb near ground level, and a relative humidity of 60% (P_{wv} = 10 mb), the fluctuation, ΔN, is

$$\Delta N = 4.5\,\Delta P_{wv} - 1.26\,\Delta T + 0.27\,\Delta P. \qquad (19.8)$$

As Equation (19.8) shows, a fluctuation in water vapor pressure has 16 times the effect on the refractive index as the same amount of fluctuation in total pressure and 3.5 times the effect as the same fluctuation in temperature. Equation (19.7) may also be used in the windows of relative transparency for submillimeter waves ($\lambda > 100$ μm, $f < 3 \times 10^6$GHz) with an error of 10 to 20 N-units.

Equation (19.7) is a function of temperature, pressure, and vapor pressure all of which are height dependent, that is, elevation (h) above the surface; thus N(h) is the *refractivity structure*. In reality, surfaces of constant refractivity are not planes, but are concentric spheres about the earth's center. In characterizing the atmospheric layers that affect radio wave propagation a *modified refractivity structure* M(h) is defined.

$$M = (n + \frac{h}{a} - 1) \times 10^6 \qquad (19.9)$$

$$M(h) = N(h) + 157h \text{ in units of M} \qquad (19.10)$$

where h is in kilometers, a is the radius of the earth (6370 km) and $1/a = 157 \times 10^{-6}$ km^{-1}.

When the lapse rate of N is less than −157 N-units per kilometer [Equation (19.10)], the slope of M becomes negative indicating a ducting condition. Figure 19-1 illustrates ducts at 1000 and 700 mb [Morrissey, personal communication, 1982].

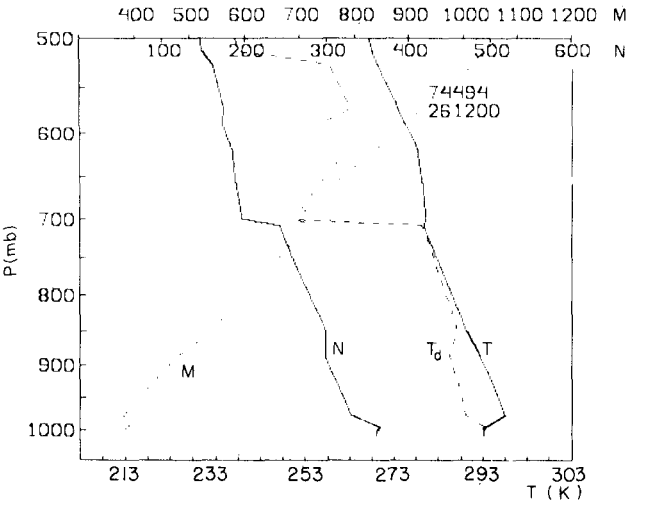

Figure 19-1. Data from Chatham, Mass. radiosonde release of 26 July 1982.

19.1.3 Standard Profiles of Refractive Modulus

The vertical distribution of the refractive modulus can be calculated from Equation (19.3) using vertical distributions of vapor pressure and temperature as a function of pressure. Under normal conditions, N tends to decrease exponentially with height. An exponential decrease is usually an accurate description for heights greater than 3 km; below 3 km, N may depart considerably from exponential behavior. The median value for the gradient dN is typically −0.0394 N/m for the first few thousand meters above ground level.

For many purposes it is desirable to have standard refractive-modulus profiles for the atmosphere. By using the equations of the model atmosphere, an exact analytical expression for the standard optical refractive modulus can be derived. A simplified approximation to this is

$$N_\infty = 273 \exp(-\frac{Z}{9.82}), (Z \leq 7.62) \qquad (19.11)$$

Z is the altitude in thousands of km.

Equation (19.11) can be differentiated to obtain the standard gradient of optical refractive modulus;

$$\frac{dN_\infty}{dZ} = 27.8 \exp(-\frac{Z}{9.82}), (Z \leq 7.62). \qquad (19.12)$$

Equations (19.11) and (19.12) may be corrected for dispersion through use of Equation (19.5).

For the radio wavelengths, it is necessary to assume a distribution of water vapor in order to obtain an expression for the refractive modulus. Assuming $P_{wv} = 10.2\,(1 - 0.064Z)$, for $Z \leq 7.62$, a simplified approximation is

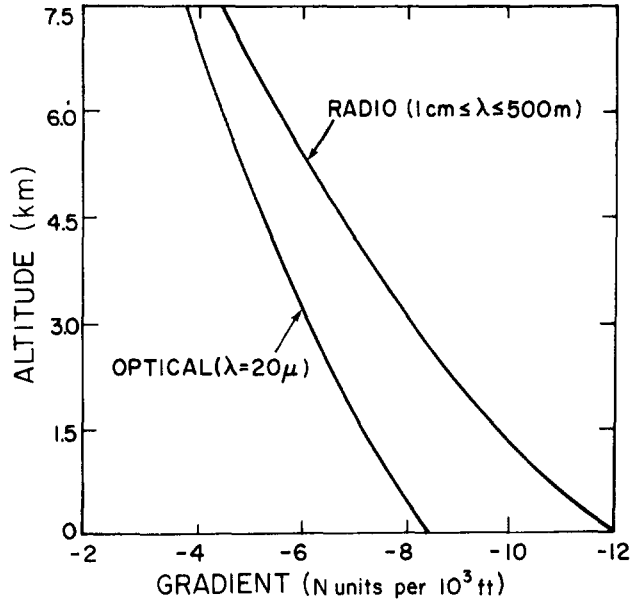

Figure 19-2. Variation of standard gradient of refractive modulus with altitude.

$$N = 316 \exp\left(-\frac{Z}{8.08}\right), (Z \leq 7.62). \quad (19.13)$$

The standard gradient of radio-wave refractive modulus is then:

$$\frac{dN}{dZ} = -39.1 \exp\left(-\frac{Z}{8.08}\right), (Z \leq 7.62). \quad (19.14)$$

Figures 19-2 and 19-3 are graphs of standard profiles calculated from Equations (19.12) through (19.14).

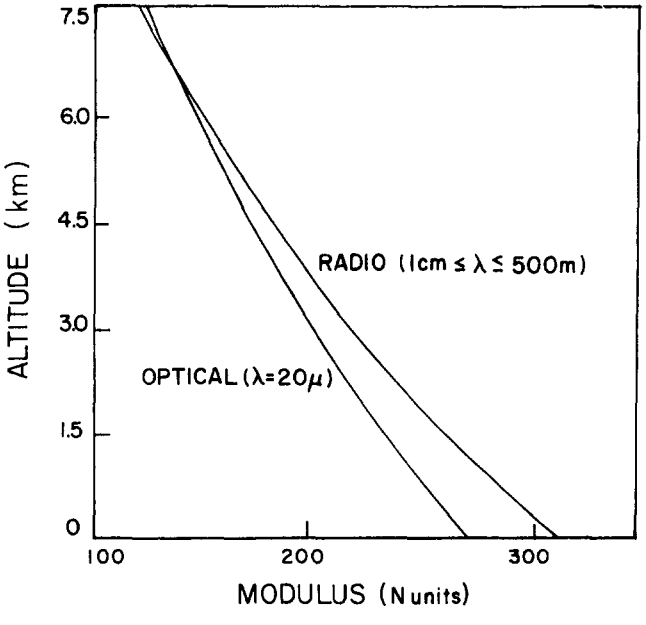

Figure 19-3. Variation of standard refractive modulus with altitude.

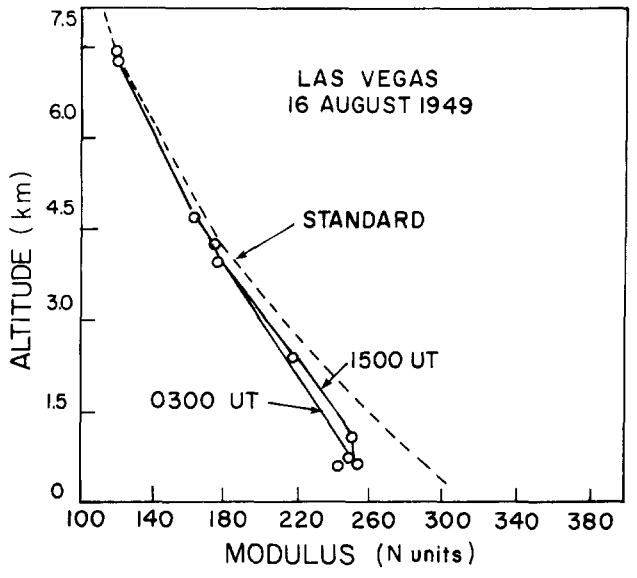

Figure 19-4. Microwave refractive modulus profile in continental tropical air mass.

19.1.4 Variations of Refractive Moduli

Actual profiles may differ markedly from the standard profiles. Figures 19-4 through 19-7 show some profiles of refractive modulus at microwave frequencies calculated from radiosonde measurements. These are considered typical for the air masses indicated. Average deviations from a model atmosphere refractive index have been studied extensively; for example, see Bean and Dutton [1968].

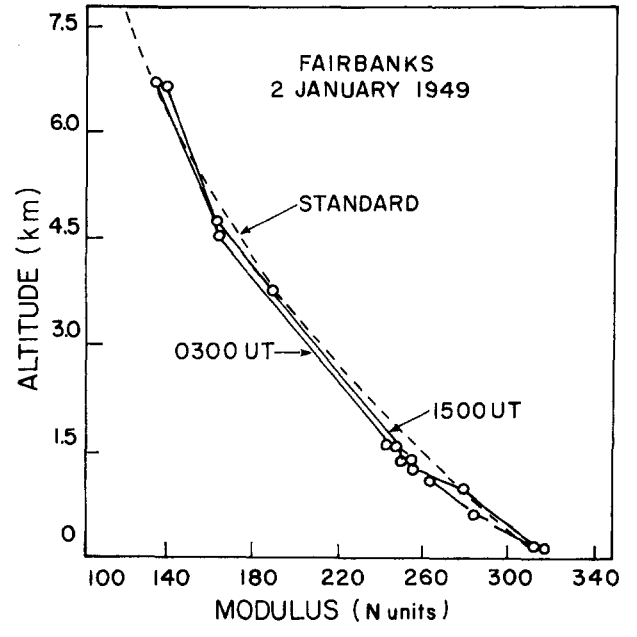

Figure 19-5. Microwave refractive modulus profile in continental polar air mass.

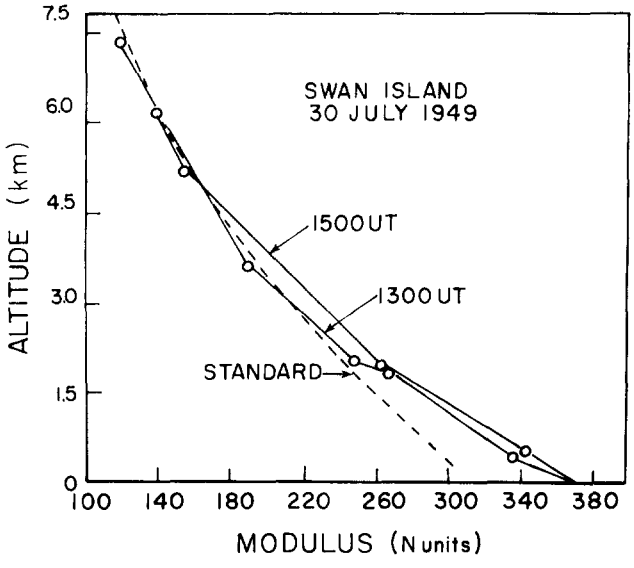

Figure 19-6. Microwave refractive modulus profile in continental polar air mass.

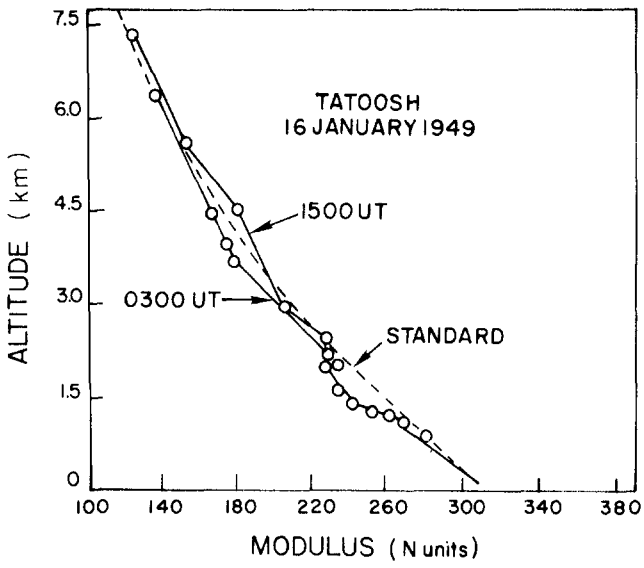

Figure 19-7. Microwave refractive modulus profile in maritime polar air mass.

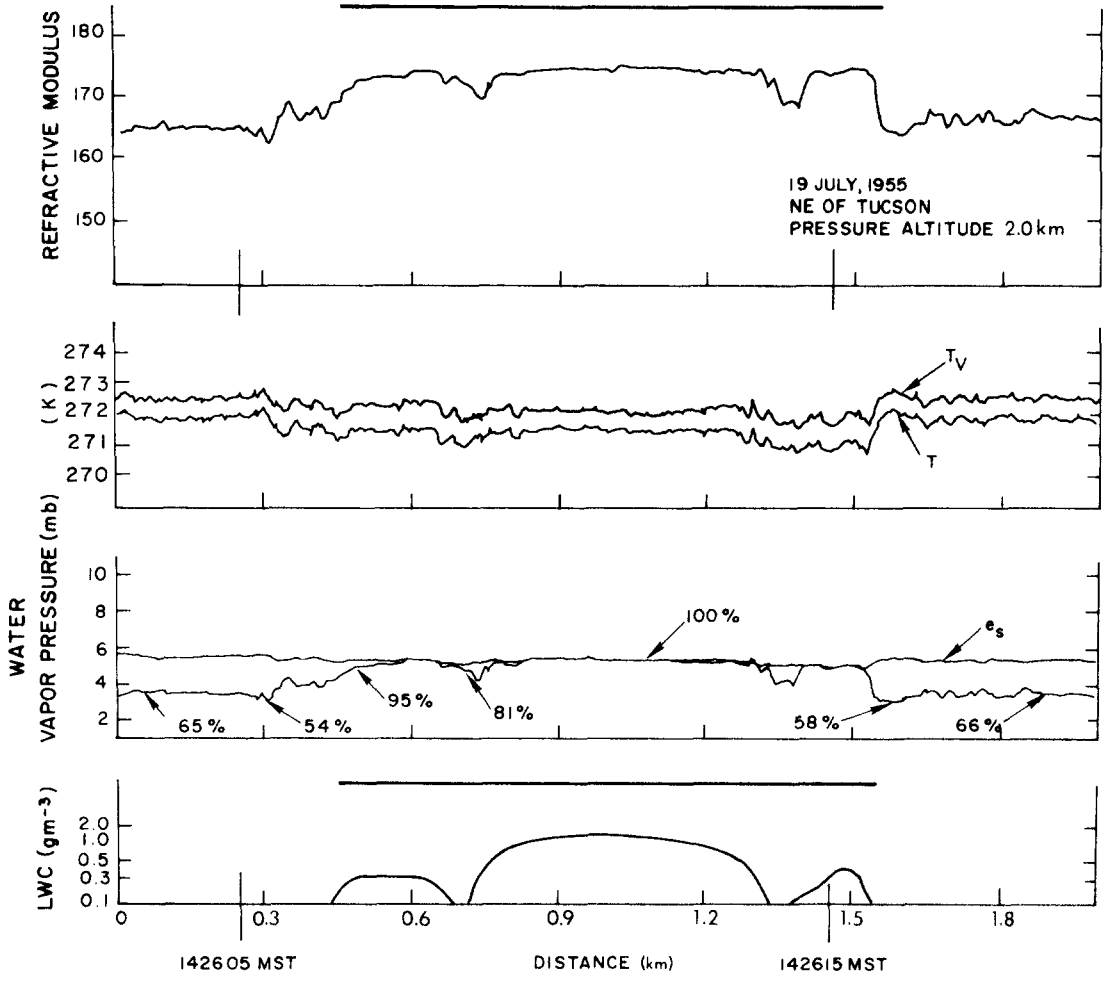

Figure 19-8. Aircraft measurements through a cumulus cloud. The heavy lines show the time during which an observer in the aircraft indicated that the plane was within the visible cloud. The calculated virtual temperature, T_v, was corrected for liquid water content; T is the measured temperature. Relative humidity in percent is shown on the ambient water-vapor pressure curve; the curve labeled e_s is the calculated saturation water-vapor pressure at the temperature encountered. The bottom curve shows the liquid water content (LWC).

Cumulus clouds are evidence of the existence of a very inhomogeneous field of water vapor within the atmosphere. Figure 19-8 shows some measurements of refractive modulus and associated parameters within a fair-weather cumulus cloud. The time response of the instruments from which refractive modulus, temperature, and water-vapor pressure were obtained was such that changes occurring in distances as small as 1.5 m could be measured. However, the instrument for measuring liquid water content had a much slower response. Figure 19-9 shows a composite cloud which summarizes data from 30 cloud passes.

Figures 19-10a and b show the average ΔN between cloud and clear air to be expected in various parts of the United States at the midseason months. The chances of having cumulus clouds at 1500 h local time for these months is also shown. Additional climatological data on ΔN and cumulus clouds is given by Cunningham [1962].

The deviations in refractive modulus are principally in the vertical direction. Regions of more or less constant gradient of the refractive modulus are called *stratified layers*. The horizontal extent of these layers may vary from a few kilometers to hundreds of kilometers depending on the meteorological processes by which they are produced. When N decreases with height inside a specific layer much faster than it does above or below the layer, the layer is said to be *super-refracting* for propagation. One cause of this is a temperature inversion. Layers of negative height-gradient of N in association with regions in which the temperature gradient is positive (or less negative) than the gradients of the layers just above and below are known as *subsidence inversion layers*. These layers generally have a large horizontal extent. Layers in close proximity to the earth's surface are strongly influenced by the local conditions of the earth's surface and for this reason show more variability than the layers described above.

In the inversion layer, the temperature may change by a few degrees in intervals of from fifty to a few hundred meters in altitude. This temperature difference accounts for a change of only a few N-units. However, an inversion usually indicates the presence of a humid air mass under a dry one. The transition from humid to dry air causes a marked change of N in the super-refracting layer, typically of 20 to 50 N-units; changes as pronounced as 80 N-units have been measured. Super-refracting layers may be clear-weather phenomena, or can be accompanied by haze (aerosols) in the lower air mass. Invariably they signify stable weather situations, such as occur when a high pressure center stagnates in an area.

The horizontal and temporal extent of super-refractive layers varies widely. In New England it may be only a few tens of kilometers. In mideastern states, the layers extend farther and may last from a half hour up to a week. In the trade-wind zones of the world, the climatic regime (manifested by steady wind directions and speeds throughout most of the year) sustains super-refracting layers, which extend a few thousand miles both east to west and north to south.

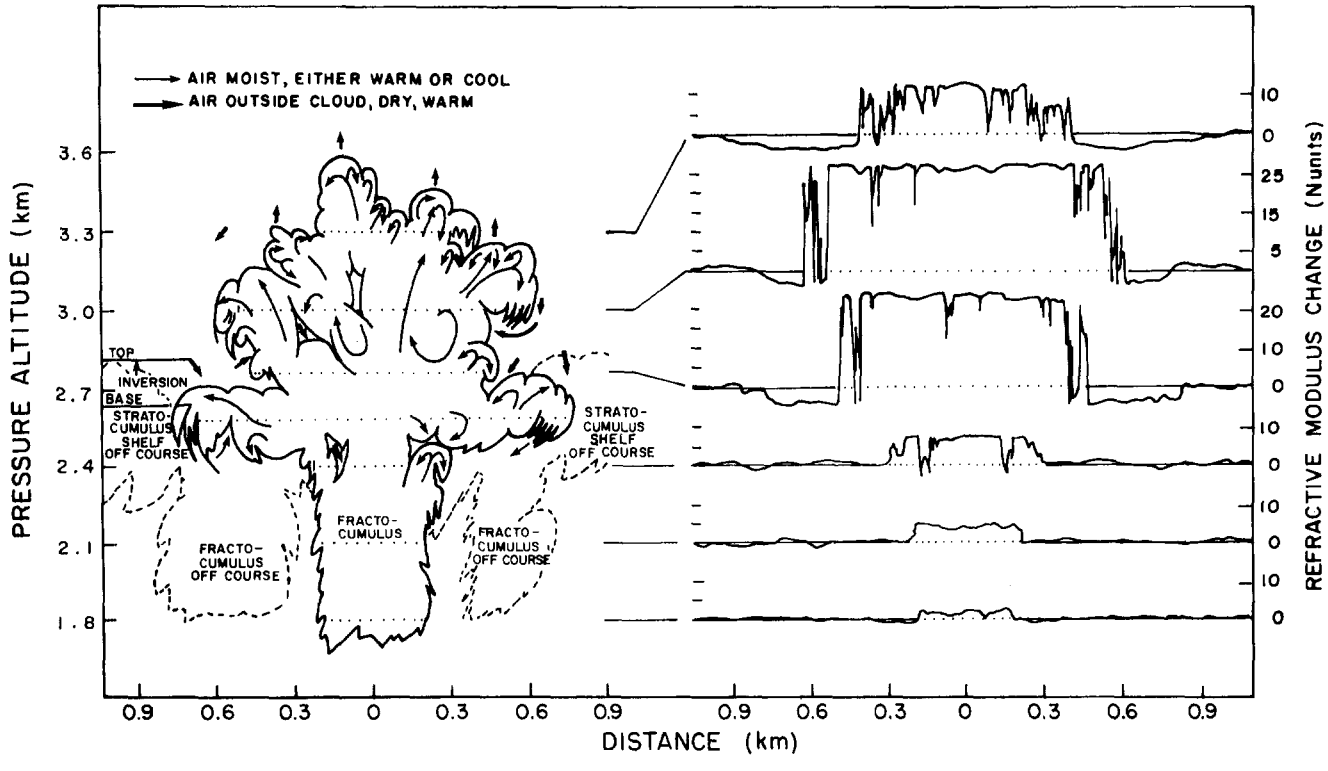

Figure 19-9. Average cloud shape cross section 90° to wind shear and average refractive modulus changes on 30 June 1955 NW of Boston, Mass.

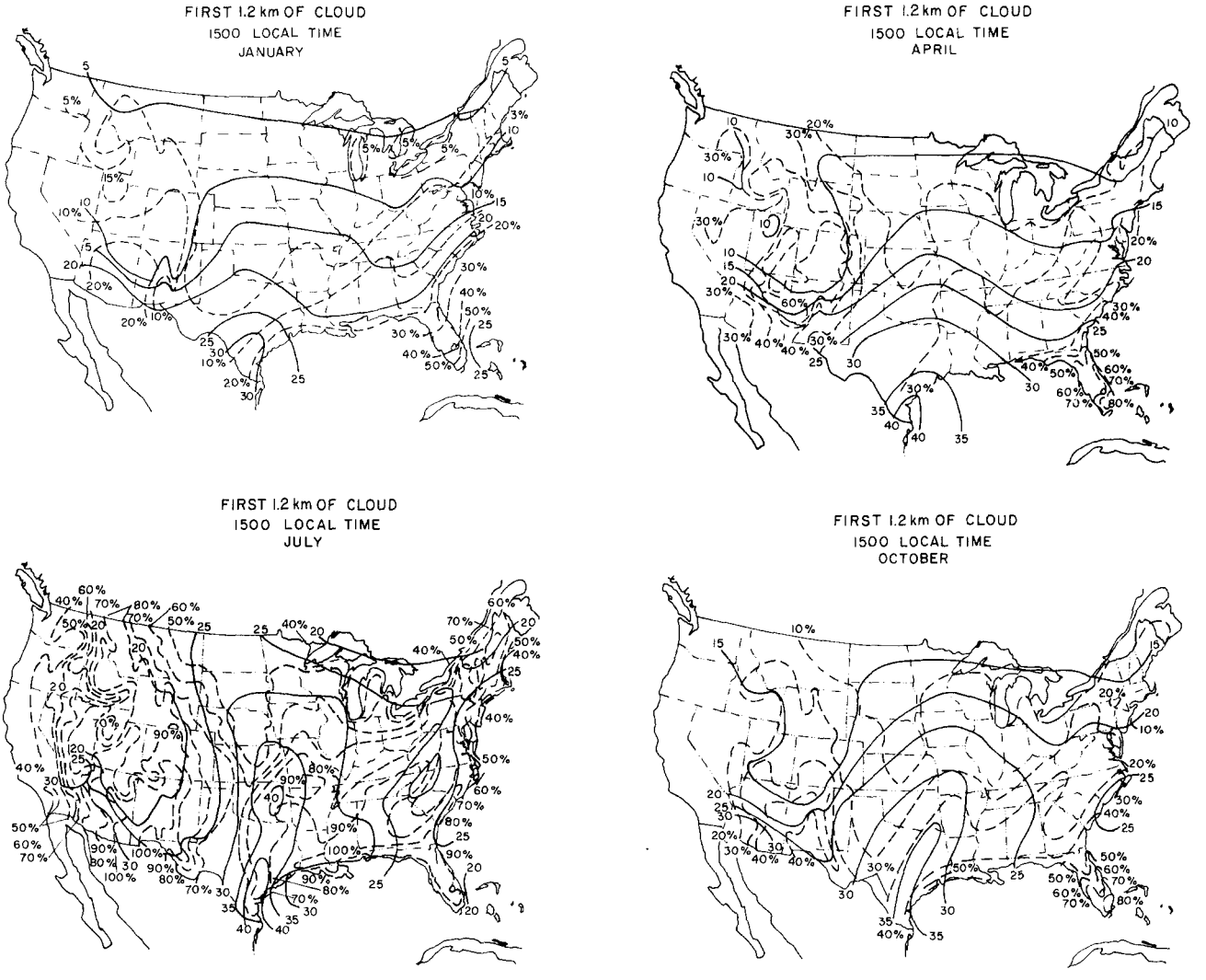

Figure 19-10. Percent frequency of cumulus and cumulonimbus cloud and ΔN, the average change in refractive modulus between the cloud and clear air for January, April, July, and October.

19.1.5 Turbulence

It has long been recognized that the effects produced by the atmosphere upon electromagnetic waves propagating through it are a measure of the nature of the atmosphere. If the atmosphere is considered as a medium with electromagnetic properties that are functions of space and time, then atmospheric properties can be investigated by measurements of wave propagation; these observations are called *remote probing*. The atmospheric (or meteorological) parameters are inferred from their influence on Equations (19.6) and (19.7); it is assumed that scattering is due to random fluctuations in the dielectric constant of the atmosphere. When fluctuations in the refractivity are of interest, they are studied via the correlation function and its Fourier transform, the spectral density. This approach is described by Tatarski [1961 and 1971], Staras and Wheelon [1959], Hufnagle and Stanley [1964], and Strohbehn [1968]. A tutorial review has been written by Dewan [1980].

A locally-homogeneous isotropic turbulent model of the atmosphere is assumed, that is, a model of well mixed random fluctuations. This model is restrictive and requires justification for each new application. One assumes the *spectral density* $\phi_n(\kappa)$ (the three dimensional spectrum of refractivity) is given by

$$\phi_n(\kappa) = 0.033\, C_n^2\, \kappa^{-11/3} \exp\left(\frac{-\kappa^2}{\kappa_m^2}\right) [\text{cm}^3] \quad (19.15)$$

where $\kappa_o < \kappa < \kappa_m$. The spatial wave number $\kappa(\text{cm}^{-1})$ is $2\pi/\ell$, ℓ is the size of the turbulent eddy or blob, κ_o is $2\pi/L_o$, L_o is the outer scale of turbulence (typically the order of 10^3 to 10^4 cm, depending on layer height), κ_m is $5.92/\ell_o(\text{cm}^{-1})$, ℓ_o is the inner scale or turbulence, and C_n is specified by Equation (19.16), that is, C_n^2 is a measure of magnitude of the mean squared fine scale gradients. Figure 19-11 shows the typical spectrum of irregularities, $\phi_n(\kappa)$

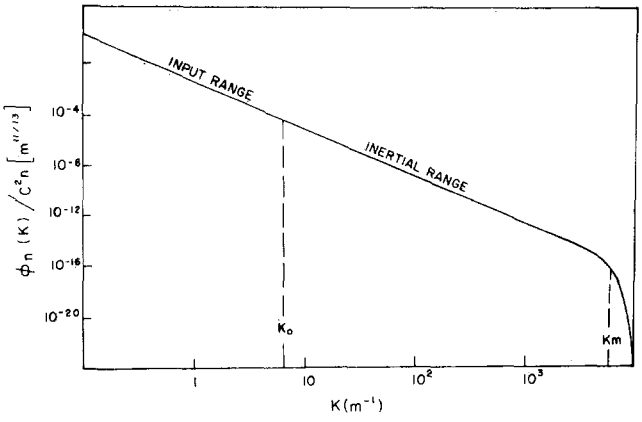

Figure 19-11. Three-dimensional spectrum of refractive index fluctuations.

and the ranges of energy input, redistribution, and dissipation. Physically, the energy is put into the turbulence from the largest scale sizes (smallest value of κ) by wind shear and convective heating; the energy-producing eddies are assumed to have a spatial wave number less then κ_o. The region between κ_o and κ_m is the redistribution (inertial) range, where energy is transferred from large edies (small k) to smaller eddies (larger κ) until viscous effects becomes important at $\kappa_m = 5.92/\ell_o$ and the energy is dissipated. Near the ground, ℓ_o is of the order of 0.1 to 1 cm.

Once the value of C_n^2 is determined, the spectral density is known. C_n^2 may be found directly from the dimensionless structure function $D_n(r)$,

$$D_n(\mathbf{r}) = \overline{[N(\mathbf{r} + \mathbf{r}_1) - N(\mathbf{r}_1)]^2} = C_n^2 r^{2/3} \quad (19.16)$$

where $N(\mathbf{r})$ is the normalized fluctuating part of the index of refraction, the bar indicates the average of the squared quantity, and $r(r \gg \ell_o)$ is the size of the inhomogenities determined from the differences in the values of N at two points $\mathbf{r}$ and $\mathbf{r}_1$.

At optical wavelengths, C_n is determined from temperature measurements alone;

$$C_n = 10^{-6}(\rho/\rho_o)C_T\ [cm^{-1/3}] \quad (19.17)$$

where ρ/ρ_o is the ratio of the average atmospheric density at a given altitude to the density at sea level. The structure constant, C_T, is

$$C_T = 2.4\ \varepsilon^{1/3}(\gamma/\beta)\ [K\ cm^{-1/3}] \quad (19.18)$$

where ε (cm^2s^{-3}) is the rate of energy per unit mass dissipated by viscous friction, γ ($K\ cm^{-1}$) is the average vertical gradient of the potential temperature, and β (s^{-1}) is the average shear or vertical gradient of the horizontal wind [Hufnagle and Stanley, 1964 or Chapter 18].

Figure 19-12 shows the average dissipation rate estimated from observed values as a function of altitude. Figures

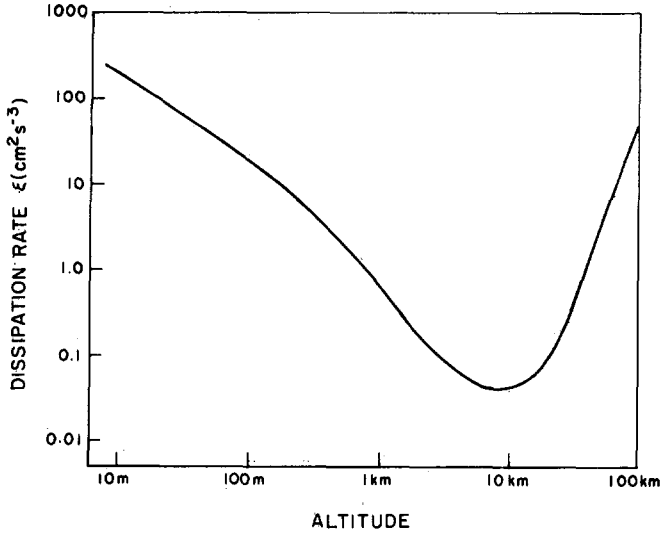

Figure 19-12. Dissipation rate ε vs altitude.

19-13 and 19-14 are plots of observed geometric-mean values of γ and β respectively as functions of altitude. The values of γ are taken from the 1966 Supplementary Atmosphere; the values of β are computed from reported wind profiles. Figure 19-15 shows C_n as a function of altitude; the values of ρ/ρ_o used to compute C_n are taken from the 1966 Supplementary Atmosphere. At radio wavelengths, Equation (19.17) cannot be used because water vapor must be considered as well as temperature [Crane, 1968, 1980].

C_n for a model atmosphere can be obtained directly from Figure 19-15. When values of ρ/ρ_o are known from radiosonde observations, C_n for the given ρ/ρ_o can be calculated by using values obtained from Figures 19-12 through 19-14 and Equations (19.17) and (19.18).

Hufnagle [1974] synthesized a model for C_n based on

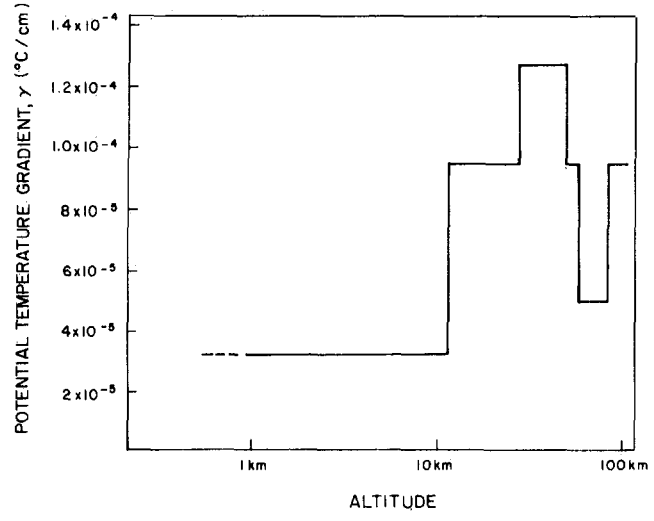

Figure 19-13. Average potential temperature gradient (γ) vs altitude.

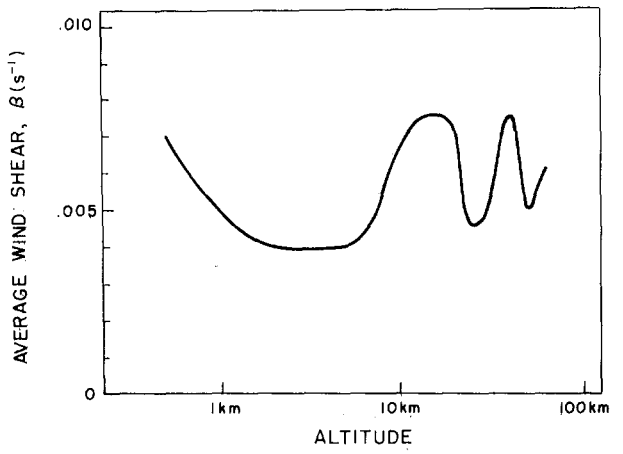

Figure 19-14. Average wind shear (β) vs altitude.

the empirical observation that the best correlation factor to correlate the scintillation spectrum and the meteorological parameter of wind speed is

$$W = \left[\frac{1}{15}\int_{5\text{ km}}^{20\text{ km}} v^2(h)dh\right]^{1/2} \quad \text{(units of m/s)} \tag{19.19}$$

for h in km

$$C_n^2 = \left\{\left[\left(2.2 \times 10^{-53}\right)h^{10}\left(\frac{W}{27}\right)^2\right]\exp\left[\frac{-h}{1000}\right] + (10^{-16})\exp\left(\frac{-h}{1500}\right)\right\}\exp\,[r(h,t)] \tag{19.20}$$

in units of $m^{-2/3}$

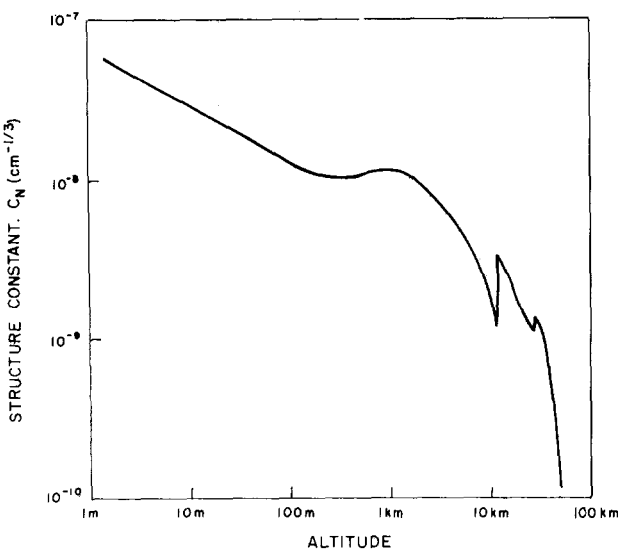

FIgure 19-15. Index of refraction structure (C_n) vs altitude.

where h is height in meters above sea level, r is a zero mean homogeneous Gaussian random variable with a covariance function given by

$$\langle r(h + h', t + \tau)\, r(h,t)\rangle = A(h'/100)e^{-\tau/5} + A(h'/2000)e^{-\tau/80} \tag{19.21}$$

The model for $C_n(h, t)$ is valid for heights between 3 and 24 km. The time interval τ is measured in minutes and $A(h',/L) = 1 - |h/L|$ for $(h') < L$ and zero otherwise; $\langle r^2\rangle = 2$ and $\langle \exp r\rangle = e = 2.7$ for cases in which fine structure is not of interest. VanZandt et al. [1981] discuss another C_n^2 model. Brown et al. [1982] and Good et al. [1982] present the correlating data. C_n^2 may be determined from radar backscatter measurements in the atmosphere; see for example, Staras and Wheelon [1959], Hardy and Katz [1969], Ottersten [1969], and Gage et al. [1978].

At radio frequencies, the mechanism responsible for backscatter and forward scatter beyond the horizon is the refractive index variation due to fluctuations in properties of the atmosphere. The ratio of the received-to-transmitted power (P_r/P_t) depends upon the integral of the scattering cross section per unit volume over the common volume defined by the antenna pattern or patterns for backscatter and forward scatter respectivity.

$$\frac{P_r}{P_t} = \frac{\lambda^2}{4\pi^2}\int_{\text{Volume}}\left(\frac{G_tG_r}{R_1^2R_2^2}\right)^2 \mu\, d^3r \tag{19.22}$$

where λ is the wavelength employed, G_t and G_r are the gains of the transmitting and receiving antennas respectively, R_1^2 and R_2^2 are the distances from the scattering volume (d^3r) to the respective antennas, and μ (a reciprocal length) is the scattering cross section per unit volume. Figure 19-16 illustrates the path geometry for Equation (19.18).

The scattering cross section per unit volume is directly related to the spectral density:

$$\mu = (\pi^2/\lambda^4)\,\phi_n(\kappa) \tag{19.23}$$

where $|\kappa|$ is $(4\,\pi/\lambda)\sin(\theta/2)$.

Scattering is not the only effect of atmospheric turbulence on the propagation of electromagnetic waves. As the waves propagate through the atmosphere, fluctuations in amplitude and phase occur. The amplitude and phase fluctuations may be described using the equations of geometrical optics or the smooth perturbation solution of the full wave equation. A summary of the solution, based on work by Tatarski [1961], is provided below.

In order to apply the geometrical optics approximation, the conditions that have to be satisfied are

$$\lambda \ll \ell_o \text{ and } (\lambda\, L)^{1/2} \ll \ell_o,$$

where λ is the wavelength of the propagating wave, ℓ_o is the inner scale of turbulence, and L is the path length over

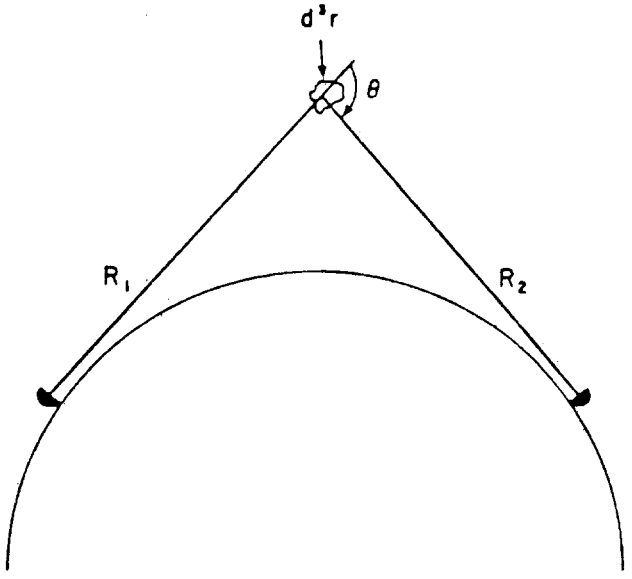

Figure 19-16. Geometry for turbulent scattering.

which the wave propagates. The *phase fluctuation* at a point r along the path is

$$S(\mathbf{r}) = k \int_o^r n(\mathbf{s})\, ds \qquad (19.24)$$

where $S(\mathbf{r})$ is the total phase change, k is $2\pi/\lambda$, $n(\mathbf{s})$ is the index of refraction in the direction of s, and ds is the element of path length. The *amplitude fluctuation* χ at point r along the path is

$$\chi = \ln\left[\frac{A(\mathbf{r})}{A_o(\mathbf{r})}\right]$$
$$\chi = \frac{1}{2k}\int_o^x \nabla_T^2\, S_1\,(\xi,y,z)d\,\xi \qquad (19.25)$$

where $A(\mathbf{r})$ is total amplitude at point $\mathbf{r}$, ∇_T^2 is the transverse Laplacian, and ξ is the direction of propagation. $S_1\,(\xi,y,z)$ is the phase fluctuation about its mean value,

$$S_1(\mathbf{r}) = k \int_o^r \delta n(\mathbf{s})\, ds \qquad (19.26)$$

where $\delta n(\mathbf{s})$ is the deviation of the index of refraction from its mean value. If n(s) depends only on altitude, then Equation (19.24) may be used to determine the average phase change by substituting the average index of refraction in the integrand

$$k \int_o^r \langle n(\mathbf{s})\rangle ds;$$ this is useful in studying refraction.

The covariance function of phase fluctuations, $C_s(\zeta)$, at two receivers that are both an equal distance L away from the transmitter and are separated from each other by a distance $\zeta = (y^2 + z^2)^{1/2}$ is

$$C_s(\zeta) = 2\pi \int_o^\infty F_s(\kappa)J_0(\kappa\zeta)\kappa dk. \qquad (19.27)$$

$J_o\,(\kappa\zeta)$ is the Bessel function and $F_s(\kappa)$ is the two dimensional Fourier transforms of $C_s(\zeta)$;

$$F_s(\kappa) = 2\,\pi\kappa^2 L\,\phi_n\,(\kappa)\ [\mathrm{cm}^2]. \qquad (19.28)$$

The covariance function of amplitude fluctuations, $C_\chi(\zeta)$, for the conditions given above is

$$C_\chi(\zeta) = 2\,\pi \int_o^\infty F_x(\kappa)J_o(\kappa\zeta)\ \kappa dk \qquad (19.29)$$

and

$$F_\chi(\kappa) = \left(\frac{\pi L^3}{6}\right)\kappa^4\phi_n(\lambda)\ [\mathrm{cm}^2]. \qquad (19.30)$$

Under restrictions that $\lambda \ll \ell_0$ and that $L \ll \ell_o^4/\lambda^3$, the smooth perturbation solution of the full wave equation leads to

$$F_s(\kappa) = \pi\kappa^2 L\left(1 + \frac{\sin\alpha}{\alpha}\right)\phi_n(\kappa)\ [\mathrm{cm}^2] \qquad (19.31)$$

and

$$F_\chi(\kappa) = \pi\kappa^2 L\left(1 - \frac{\sin\alpha}{\alpha}\right)\phi_n(\kappa)\ [\mathrm{cm}^2] \qquad (19.32)$$

where α is $\kappa^2 L/k$. These restrictions limit the validity of Equations (19.31) and (19.32) to wavelengths in the millimeter and optical regions and to relatively short paths, although in certain cases these restrictions may be relaxed, for example for $\lambda \geq \ell_o$. C and F can be measured only over a finite range of values of κ, therefore a complete knowledge of C or of F is not possible.

19.2 ATTENUATION AND BACKSCATTERING

Scattering and attenuation are usually complicated functions of particle size and dielectric properties. The square root of the dielectric constant m is

$$\sqrt{m} \equiv n - i\,\kappa, \qquad (19.33)$$

where n is the phase *refractive index*, κ is the *absorption index* of the medium, and i is $\sqrt{-1}$.

In describing the properties of the particles, it is convenient to use the parameter K, defined by

$$K \equiv \frac{m - 1}{m + 2} \tag{19.34}$$

When the particles are small in comparison with the transmitted wavelength, the Rayleigh approximation holds, and both the backscatter and the absorption are simple functions of K. In this special case, backscatter is proportional to $|K|^2$, and attenuation is proportional to the imaginary part of minus K or $(\mathrm{Im}(-K))$.

For water, $|K|^2$ is practically constant and equals 0.93 over a wide range of temperatures and wavelengths in the centimeter range. Similarly $|K|^2 = 0.176$ for ice of normal density (0.917 g/cm^2) and centimeter wavelengths. However, the imaginary part of K can vary significantly with temperature and wavelength, and both $(K)^2$ and $(\mathrm{Im}(-K))$ vary with frequency at millimeter and submillimeter wavelengths. Unfortunately, measurements have not been made at every possible combination of temperature and wavelength, and there is no single expression relating all the variables. To obtain the real and imaginary parts of K at the desired temperature and wavelength, the reader is referred to the computer program written by Ray [1972], as corrected by Falcone et al. [1979]. This program interpolates between measured values.

19.2.1 Backscattering and Attenuation Cross Sections

The echo power returned by a scattering particle is proportional to its *backscattering cross section*, σ. The power removed by an attenuating particle is proportional to the *total absorption cross section*, Q_t. *The size parameter* (electrical size) is $\pi D/\lambda$; D is the particle diameter and λ the wavelength of the incident radiation. When the diameter of the scattering or attenuating particle is small with respect to λ, the backscattering and total absorption cross sections may be expressed with sufficient accuracy by the Rayleigh approximation.

For spherical particles, if $D/\lambda < 0.2$,

$$\sigma = \frac{\pi^5 |K|^2 D^6}{\lambda^4} \ [\mathrm{cm}^2] \tag{19.35}$$

For particles with $\pi D/\lambda > 0.2$, σ should be computed from the equations of the Mie theory of scattering [Battan, 1959]. Figures 19-17 and 19-18 show normalized backscattering cross section $(4\sigma/\pi D^2)$ for ice and for water versus the size parameter, computed from the exact Mie equations. The normalized curve for ice is invariant with wavelength in the microwave region; the normalized curve for water is for a temperature of 273 K and a 3.2-cm wavelength. As these figures show, ice spheres equal to or larger than the wavelength may scatter more than an order of magnitude greater than water spheres of the same size. This is confirmed by experimental measurements.

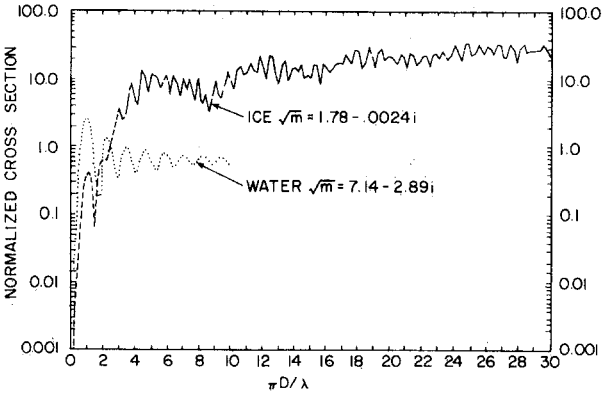

Figure 19-17. Calculated values of the normalized $(4\sigma/\pi D^2)$ backscatter cross section for water at 3.21 cm and 273 K and for ice at wavelengths from 1 to 10 cm.

Measurements at 5 cm wavelength indicate that the back-

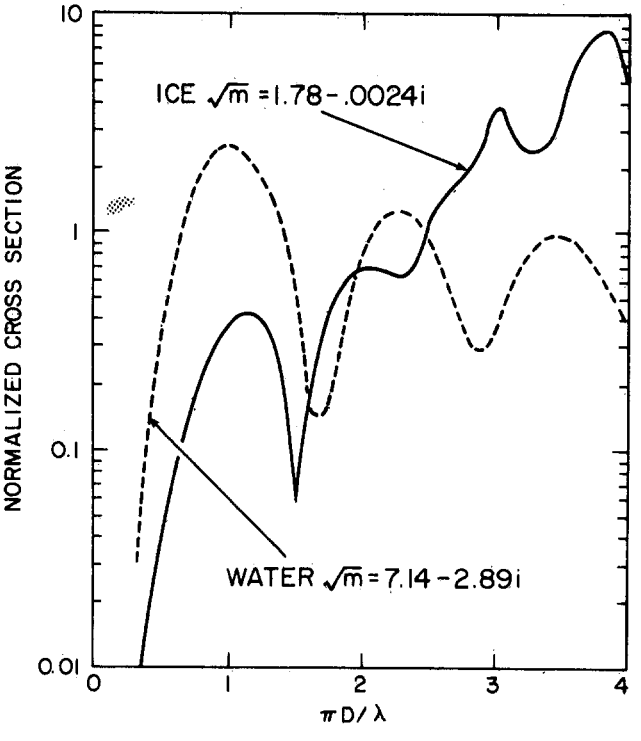

Figure 19-18. Calculated values of the normalized $(4\sigma/\pi D^2)$ backscatter cross section for water at 3.21 cm and 273 K and for ice at wavelengths from 1 to 10 cm. (Detail of Figure 19-17)

scattering of so-called "spongy" hail (a mixture of ice and water) is 3 to 4 dB above that of the equivalent all-water spheres and at least 10 dB above that of the equivalent solid ice spheres [Atlas et al., 1964]. Because of the variabilities of sizes, shapes, and liquid water content of hail, no general rules concerning backscattering and attenuation cross sections for hail can be made. As a first approximation, however, the ice curve of Figures 19-17 and 19-18 may be used.

For spherical particles, if $\pi D/\lambda < 0.1$,

$$Q_t = \frac{\pi^2 D^3}{\lambda} \text{Im}(-K) + \frac{2}{3}\sigma \text{ [cm}^2\text{]}. \quad (19.36)$$

When $\pi D/\lambda > 0.1$, Q_t must also be computed from the exact Mie equations. Several computer programs are available to compute the total attenuation caused by any distribution of water and/or ice particles. [See, for example, Falcone et al., 1979.]

19.2.2 Reflectivity

The average echo power returned by a group of randomly distributed scattering particles is proportional to their reflectivity η. *Reflectivity* is defined as the summation of the backscatter cross sections of the particles over a unit volume: $\eta \equiv \Sigma\sigma$. When the backscattering particles are spheres and are small enough with respect to wavelength so that the Rayleigh approximation can be used (that is, $\pi D/\lambda < 0.2$), the reflectivity is proportional to the radar reflectivity factor Z which is the summation over a unit volume of the sixth power of the particle diameters, $Z = \Sigma D^6$. Summation over a unit volume of Equation (19.35) gives

$$\Sigma\sigma = \eta = \frac{\pi^5 |K|^2 Z}{\lambda^4} \times 10^{-12} \text{ [cm}^{-1}\text{]} \quad (19.37)$$

for Z in conventional units of mm^6 and m^{-3} and λ in centimeters.

When the particles are larger than Rayleigh size or composed of ice or water-ice mixtures, it is common practice to measure the radar reflectivity and express it in terms of an equivalent reflectivity factor Z_e. Substituting $|K|^2 = 0.93$ (water at normal atmosphere temperature, wavelength in the centimeter range) in Equation (19.38)

$$Z_e = 3.5 \times 10^9 \lambda^4 \eta \text{ (mm}^6 \text{ m}^{-3}\text{)}. \quad (19.38)$$

Thus, Z_e is simply the ΣD^6 required to obtain the observed signal, if all the drops were acting as Rayleigh scatterers.

Because Z is a meteorological parameter that depends only on the particle size distribution and concentration, it is useful to express Z as a function of either the precipitation rate R or the mass of liquid water (or water equivalent of the ice content) M. The returned radar signal can then be related to Z, and through Z to R or M. Numerous Z-R and Z-M relations have been proposed. They vary geographically, seasonally, and by type of precipitation.

The following Z-R relations are typical of those most often found in the literature:

$Z = 200\ R^{1.6}$	widespread stratiform rain
$Z = 110\ R^{1.47}$	drizzle
$Z = 460\ R^{1.61}$	thunderstorm
$Z = 145\ R^{1.64}$	orographic
$Z = 314\ R^{1.42}$	monsoon

The scattering properties of snow are complicated by the many forms in which snow can occur, either as single ice crystals or aggregates of such crystals. The following relationships are reasonable averages of observations:

$$Z = 500\ R^{1.6} \quad \text{for single crystals}$$

and

$$Z = 2000\ R^{2.0} \quad \text{for aggregates}$$

where R is the snowfall rate in millimeters of water per hour.

Measurements by Boucher [1981] relating the reflectivity to the rate of snow accumulation suggest that a relation of the form

$$Z = A\ S^{2.0}$$

where S is the snowfall rate in millimeters of snow per hour, gives good agreement between measured radar reflectivity and measured snowfall accumulation. Boucher found that A varied between 6×10^{-3} to 2×10^{-2} when S was expressed in millimeters per hour. This variability is due to the variability of the density of snow, which ranges over an order of magnitude.

Clouds composed of water particles scatter very poorly at centimeter wavelengths, due to the relatively small size of the water droplets. High-power radars operating at millimeter wave lengths can detect water clouds at short ranges. An empirical Z-M relation for water clouds is

$$Z = 0.048M^2$$

where M, the water content, is in grams per cubic meter.

Table 19-1. Attenuation (db/km) at 293 K.

Precipitation	Wavelength (cm)														
Rate (mm/h)	0.03	0.05	0.1	0.15	0.2	0.25	0.3	0.5	0.8	1.0	2.0	3.0	5.0	6.0	15.0
0.25	0.867	0.900	0.874	0.773	0.656	0.539	0.434	0.179	0.0634	0.0381	0.685 $\times 10^{-2}$	0.231 $\times 10^{-2}$	0.657 $\times 10^{-3}$	0.434 $\times 10^{-3}$	0.631 $\times 10^{-4}$
1.25	2.31	2.43	2.51	2.41	2.22	1.99	1.74	0.919	0.374	0.232	0.0449	0.0134	0.304 $\times 10^{-2}$	0.191 $\times 10^{-2}$	0.249 $\times 10^{-3}$
2.50	3.51	3.71	3.90	3.83	3.63	3.34	3.01	1.77	0.783	0.497	0.104	0.0311	0.618 $\times 10^{-2}$	0.374 $\times 10^{-2}$	0.454 $\times 10^{-3}$
5.00	5.35	5.65	6.01	6.02	5.83	5.49	5.08	3.29	1.60	1.05	0.239	0.0750	0.0132	0.758 $\times 10^{-2}$	0.829 $\times 10^{-3}$
12.50	9.35	9.86	10.59	10.80	10.69	10.33	9.81	7.13	3.94	2.70	0.698	0.245	0.0399	0.0209	0.186 $\times 10^{-2}$
25.00	14.27	15.03	16.18	16.67	16.70	16.38	15.81	12.36	7.51	5.38	1.52	0.591	0.100	0.0488	0.348 $\times 10^{-2}$
50.00	21.78	22.90	24.68	25.61	25.89	25.70	25.14	20.89	13.87	10.37	3.23	1.38	0.265	0.124	0.661 $\times 10^{-2}$
100.00	33.22	34.85	37.55	39.18	39.84	39.96	39.50	34.54	24.83	19.40	6.66	3.09	0.706	0.338	0.0128
150.00	42.48	44.51	47.93	50.16	51.10	51.54	51.22	45.94	34.46	27.59	10.06	4.86	1.24	0.613	0.0190

Table 19-2. Temperature correction factor for representative rains.

Precipitation Rate mm/h	Wavelength cm	Temperature (K)				
		273	283	293	303	313
0.25	0.03	1.0	1.0	1.0	1.0	1.0
	0.1	0.99	0.99	1.0	1.01	1.02
	0.5	1.02	1.01	1.0	1.0	1.0
	1.25	1.09	1.02	1.0	1.0	0.99
	3.2	1.55	1.25	1.0	0.81	0.65
	10.0	1.72	1.29	1.0	0.79	0.64
2.5	0.03	1.0	1.0	1.0	1.0	1.0
	0.1	1.0	1.0	1.0	1.0	1.01
	0.5	1.01	1.01	1.0	0.99	0.98
	1.25	0.95	0.96	1.0	1.05	1.10
	3.2	1.28	1.14	1.0	0.86	0.72
	10.0	1.73	1.30	1.0	0.79	0.64
12.5	0.03	1.0	1.0	1.0	1.0	1.0
	0.1	1.0	1.0	1.0	1.0	1.01
	0.5	1.02	1.01	1.0	0.99	0.97
	1.25	0.96	0.97	1.0	1.04	1.07
	3.2	1.04	1.03	1.0	0.95	0.88
	10.0	1.74	1.30	1.0	0.79	0.63
50.0	0.03	1.0	1.0	1.0	1.0	1.0
	0.1	1.0	1.0	1.0	1.0	1.01
	0.5	1.02	1.01	1.0	0.98	0.97
	1.25	0.99	0.99	1.0	1.02	1.04
	3.2	0.91	0.96	1.0	1.01	1.01
	10.0	1.75	1.31	1.0	0.78	0.62
150.0	0.03	1.0	1.0	1.0	1.0	1.0
	0.1	1.0	1.0	1.0	1.0	1.01
	0.5	1.03	1.01	1.0	0.98	0.97
	1.25	1.01	1.0	1.0	1.0	1.01
	3.2	0.88	0.95	1.0	1.04	1.06
	10.0	1.72	1.31	1.0	0.78	0.62

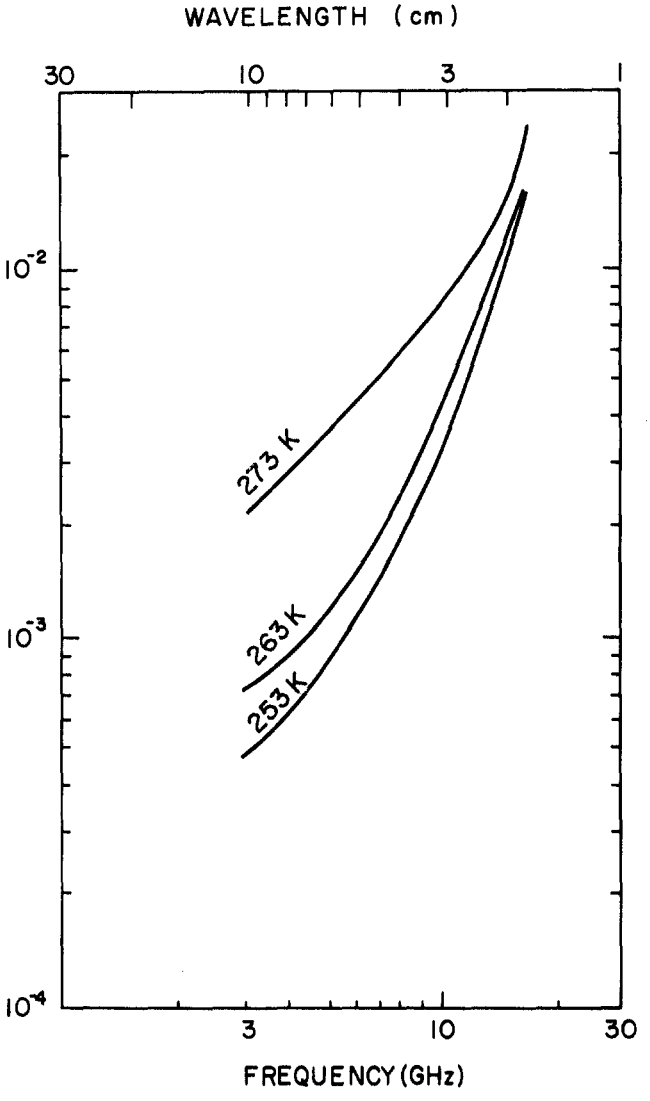

Figure 19-19. Theoretical attenuation due to snowfall of 10 mm of water content per hour as a function of wavelength and temperature.

19.2.3 Attentuation by Precipitation

Attenuation by rain is a function of drop size distribution, temperature and wavelength. Theoretical computations [Dyer and Falcone, 1972] indicate that for a given rainfall rate, wavelength and temperature, the variations in drop size distribution can cause deviations in average attenuation of between 4% and 33%. For comparison, measured attenuations are accurate to no more than ± 20% in general.

Table 19-1 gives the theoretical attenuation, for a wide range of rainfall rates and wavelengths, assuming a constant temperature of 293 K and an exponential distribution of drop sizes. Table 19-2 gives the attenuation correction factor for a range of rain rates and temperatures.

Figure 19-19 shows the theoretical maximum attenuation coefficients assuming a maximum snowfall rate 10 mm of water per hour. Because snowfall rates seldom exceed 3 mm of water per hour, attenuation due to snow should generally be one-third or less the value.

19.2.4 Total Attenuation

In addition to attenuation caused by precipitation particles, microwave and millimeter wave transmission is affected by atmospheric gases, water vapor, and cloud particles. Table 19-3 gives the attenuation as a function of wavelength for molecular oxygen at 293 K, and Table 19-4 gives correction factors for temperature differing from 293 K. Table 19-5 does the same for water vapor attenuation. Computer programs have been written [see, for example, Falcone et al., 1979] to calculate the total attenuation at any frequency, for any input atmospheric condition. Figure 19-20 is an example of the output from one such program.

The solid line (curve A) shows the attenuation at stand-

Table 19-3. Attenuation due to molecular oxygen at a temperature of 293 K and a pressure of 1-atmosphere.

Wavelength (cm)	Attenuation (dB km)
10.0	6.5×10^{-3}
7.5	7.0×10^{-3}
3.2	7.2×10^{-3}
1.8	7.5×10^{-3}
1.5	8.5×10^{-3}
1.25	1.4×10^{-2}
0.8	7.5×10^{-2}
0.7	1.9×10^{0}

Table 19-4. Correction factors for oxygen attenuation.

Temperature (K)	Correction Factor*
293	$1.00\ P^2$
273	$1.19\ P^2$
253	$1.45\ P^2$
233	$1.78\ P^2$

*P is pressure in atmospheres.

Table 19-5. Water-vapor attenuation in dB per kilometer.*

Wavelength (cm)	Temperature			
	293 K	273 K	253 K	233 K
10	$7\ PW \times 10^{-5}$	$8\ PW \times 10^{-5}$	$9\ PW \times 10^{-5}$	$10\ PW \times 10^{-5}$
5.7	$2.4\ PW \times 10^{-4}$	$2.7\ PW \times 10^{-4}$	$3.0\ PW \times 10^{-4}$	$3.4\ PW \times 10^{-4}$
3.2	$7\ PW \times 10^{-4}$	$8\ PW \times 10^{-4}$	$9\ PW \times 10^{-4}$	$10\ PW \times 10^{-4}$
1.8	$4.3\ PW \times 10^{-3}$	$4.8\ PW \times 10^{-3}$	$5.0\ PW \times 10^{-3}$	$5.4\ PW \times 10^{-3}$
1.24	$2.2\ PW \times 10^{-2}$	$2.33\ PW \times 10^{-2}$	$2.46\ PW \times 10^{-2}$	$2.61\ PW \times 10^{-2}$
0.9	$9.5\ PW \times 10^{-3}$	$1.04\ PW \times 10^{-2}$	$1.14\ PW \times 10^{-2}$	$1.26\ PW \times 10^{-2}$

*P is pressure in atmospheres and W is water-vapor content in grams per cubic meter.

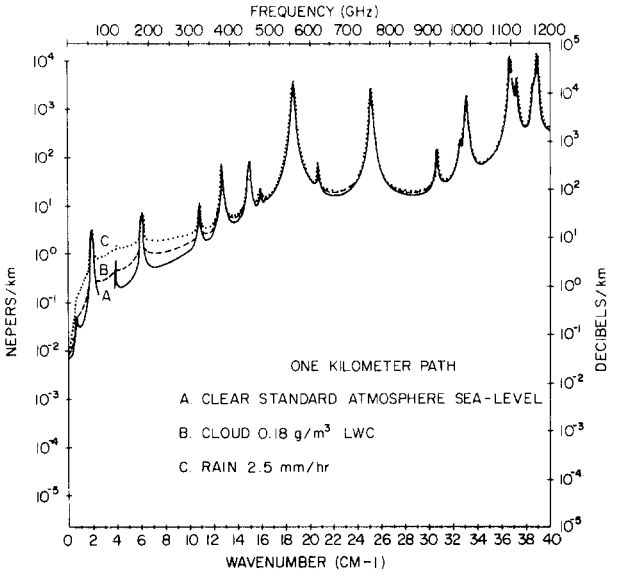

Figure 19-20. Attenuation vs frequency for a clear standard atmosphere, a cloud of 0.18g/m^3 LWC, and a 2.5 mm/h rain rate for a 1 km horizontal path.

ard sea level conditions on a clear day. The peaks in the curve correspond to absorption lines for oxygen and water vapor. In general, there is a steady increase in attenuation with increasing frequency. Absorption because of atmospheric gases is negligible at centimeter wave lengths (below 30 GHz). The dashed line (curve B) shows the attenuation caused by cloud with a liquid water content of 0.18 g m^{-3}. This is a typical value for non-precipitating stratus or altostratus clouds. The dotted line (curve C) shows the attenuation caused by rain with an intensity of 2.5 mm/hr, assuming a simple exponential drop size distribution. This is a moderate rainfall typical of stratiform situations.

Clouds and precipitation are important factors affecting attenuation of frequencies below 300 GHz. The cloud liquid water content and the rainfall rate are critical parameters to be entered into the computation. Although Figure 19-20 can be useful in giving rough estimates of the attenuation, it is necessary to compute the attenuations for the desired range of atmospheric conditions at the electromagnetic wavelength of interest when predicting the performance of a system.

REFERENCES

Atlas, D., K.R. Hardy, J. Joss, "Radar Reflectivity of Storms Containing Spongy Hail,"*J. Geophys. Res.*, **69:** 1955, 1964.

Battan, L.J., *Radar Meteorology*, The University of Chicago Press, p. 33, 1959.

Bean, B.R. and E.J. Dutton, *Radio Meteorology*, Dover, Mineola, New York, 1968.

Boucher, R.J., "Determination by Radar Reflectivity of Short-Term Snowfall Rates During a Snowstorm and Total Storm Snowfall," *Proceedings 20th Conference on Radar Meteorology, Boston, Nov 30-Dec 3, 1981*, American Meteorology Society, Boston, Mass., 1981.

Brown, J.H., R.E. Good, P.M. Bench, and G. Foucher, "Sonde Experiments for Comparative Measurements of Optical Turbulence," AFGL GR-82-0079, ADA118740, 1982.

Crane, R., "Monostatic and Bistatic Scattering from Thin Turbulent Layers in the Atmosphere," Lincoln Lab. Tech. Note 1968-34, ESD-TR-68267, 1968.

Crane, R.K., "A Review of Radar Observations of Turbulence in the Lower Statosphere," *Radio Sci.*, **15:** 177, 1980.

Cunningham, R.M., "Cumulus Climatology and Refractive Index Studies II," *Geophys. Res. Papers*, No. 51, AFCRL, 1962.

Dewan, E.M., "Optical Turbulence Forecasting: A Tutorial," AFGL TR-80-0030, ADA086863, 1980.

Dyer, R.M. and V.J. Falcone, "Variability in Rainfall Rate-Attenuation Relations," Prep, *15 Radar Meteorology Conference*, p. 353, 1972.

Edlen, B., "Dispersion of Standard Air," *J. Opt. Soc. Am.*, **43:**339, 1953.

Falcone, V.J., L.W. Abreu, and E.P. Shettle, "Atmospheric Attenuation of Millimeter and Submillimeter Waves: Model and Computer Code," AFGL TR-79-0253, ADA084485 1979.

Gage, K.S., T.E. VanZandt, and J.L. Green, "Vertical Profiles of Cn^2 in The Free Atmosphere: Comparison of Model Calculations with Radar Observations," *18th Conference on Radar Meteorology, Atlanta, GA, 28-31 March 1978*, American Meteorology Society, Boston, Mass., 1978.

Good, R.E., B. Watkins, A. Quesada, J.H. Brown, and G. Lariot, "Radar and Optical Measurements of Cn^2," *App. Optics*, **21:**2929, 1982.

Gunn, K.L.S. and T.W.R. East, "The Microwave Properties of Precipitation Particles," *Quart. J. Roy. Meteorol. Soc.*, **80:**522, 1954.

Hardy, K.R. and I. Katz, "Probing the Clear Atmosphere with High Power High Resolution Radars," *PROC. IEEE*, **57:**468, 1969.

Hufnagle, R.E. and N.R. Stanley, "Modulation Transfer Function Associated with Image Transmission Through Turbulent Media," *J. Opt. Soc. Am.*, **54:** 52, 1964.

Hufnagle, R.E., "Variations of Atmospheric Turbulence," *Digest of Technical Papers*, Topical Meeting on Optical Propagation Through Turbulence July 9-11, 1974. Optical Society of America, Washington, D.C., 1974.

Liebe, H.J., *Atmospheric Water Vapor* p. 143–202, edited by A. Deepak, T.D. Wilkinson, and A.L. Schemeltekopf, Academic Press, New York, 1980.

Medhurst, R.G., "Rainfall Attenuation of Centimeter Waves: Comparison of Theory and Measurement," *IEEE Trans. Antennas and Propagation*, **AP-13:**550, 1965.

Ottersten, H., "Radar Backscatter from the Turbulent Clear Atmosphere," *Radio Sci.*, **4:**1251, 1969.

Ray, P.S., "Broadband Complex Refractive Indices of Ice and Water," *Appl. Opt.*, **11:** 1836–1844, 1972.

Staras, H. and A.D. Wheelon, "Theoretical Research on Tropospheric Scatter Propagation in the United States 1954–1957," *IEEE Trans. Antennas and Propagation*, **AP-7:**80, 1959.

Strohnbehn, J.W., "Line of Sight Wave Propagation Through the Turbulent Atmosphere," *PROC. IEEE*, **56:**1301, 1968.

Tatarski, V.I., *Wave Propagation in a Turbulent Media*, Chapters 3, 6 and 7, McGraw-Hill, New York, 1961.

Tatarski, V.I., *The Effects of the Turbulent Atmosphere on Wave Propagation*, National Science Foundation, TT-68-50464, 1971.

VanZandt, T.E., K.S. Gage, and J.M. Warnock, "An Improved Model for the Calculation of Profiles of C_n^2 and E in the Free Atmosphere from Background Profiles of Wind, Temperature and Humidity," *Proceedings 20th Conference on Radar Meteorology, Boston, Mass., Nov 30–Dec 3, 1981*, American Meteorology Society, Boston, Mass., 1981.